The Facile Synthesis of Branch-Trunk Ag Hierarchical Nanostructures and Their Applications for High-Performance H_2O_2 Electrochemical Sensors

Yan Zhang [1], Meiqiong Chen [1], Zhiquan Cai [1], Min Zhang [2], Peng Liu [2] and Faliang Cheng [2,*]

[1] Department of City and Environmental Sciences,
College of Science and Technology of Dongguan of City College, Dongguan 523419, China;
zhangyan@ccdgut.edu.cn (Y.Z.); chenmq@ccdgut.edu.cn (M.C.); caizq@ccdgut.edu.cn (Z.C.)

[2] Guangdong Engineering and Technology Research Center for Advanced Nanomaterials,
School of Environment and Civil Engineering, Dongguan University of Technology,
Dongguan 523808, China; mindear@dgut.edu.cn (M.Z.); liupeng@dgut.edu.cn (P.L.)

[*] Correspondence: chengfl@dgut.edu.cn; Fax: +86-769-2238-2017

Abstract: A novel branch-trunk Ag hierarchical nanostructure was synthesized via a galvanic replacement reaction combined with microwave-assisted synthesis using Te nanowire as a sacrificial template. The Te nanowire was synthesized via a hydrothermal process. We further investigated the potential application of the obtained hierarchical nanostructures in electrochemical sensor analysis. The results showed that the as-prepared sensor exhibited a wide linear range with 0.05 μM to 1.925 mM (R = 0.998) and the detection limit was estimated to be 0.013 μM (S/N = 3). These results indicate the branch-truck Ag hierarchical nanostructures are an excellent candidate material for sensing applications.

Keywords: branch-truck Ag; hierarchical nanostructure; H_2O_2; electrochemical sensor

1. Introduction

Recently, three dimensional (3D) hierarchical nanostructure have provoked considerable interest due to their rich architectures, distinct properties and various novel applications [1–4]. Controlled synthesis of hierarchical nanostructure is highly desirable, owing to their structure merits. Among the myriad of possible nanostructures, branch-truck nanostructures have been studied in recent years because a great deal of branch nanostructure on a nanowire backbone could provide an even higher surface-to-volume ratio compared to single nanowires. For example, Her et al. proposed a simple two-step thermal vapor transport process to prepare brush-like p-Te/SnO_2 hierarchical nanostructures, which were used to detect NH_3 and exhibited excellent catalytic behavior [5]. Khoang et al. designed a branch-truck hierarchical SnO_2/ZnO nanostructure by combining a thermal evaporation method and a hydrothermal approach. These SnO_2/ZnO hierarchical nanostructures were systematically investigated for ethanol-sensing. These results revealed that the electrochemical sensors based on hierarchical nanostructures showed high sensibility and selectivity [6].

H_2O_2 is widely used in fields such as organic synthesis [7], environmental detection [8], biology [9], clinical [10], pharmaceutical [11], food production [12], sterilization [13] and so on [14,15]. In particular, it plays a role of considerable importance in the metabolic processes of organisms [16]. Therefore, it is critically important to develop an accurate, fast and reliable method for the detection of H_2O_2. Compared with other analytical methods for detecting of H_2O_2 [17–21], electrochemical sensors have become one of the hottest topics due to their higher sensitivity, simpler operation and lower cost [22–24] However, direct reduction of H_2O_2 at bare electrodes show poor sensitivity, low selectivity and poor

reproducibility. Because of the high electrochemically active area as well as excellent electronic transfer capability, metal nanomaterials have been tried out as sensing materials to modify the electrode surface for developing H_2O_2 sensors with high sensitivity and good selectivity.

As a typical noble nanomaterial, Ag nanomaterial exhibits excellent conductivity as well as high catalytic properties. This was because nanoscale Ag show a rapid specific surface area increase and more atoms exposed on the surface make for increased active sites. In the catalytic decomposition of H_2O_2, Ag nanomaterials could accelerate the electron transfer rate, reduce the reaction energy and amplify the detection signal. For example, we have reported high sensitivity H_2O_2 sensors based on a perpendicular Ag nanowires array [25]. The catalytic properties of nanomaterials are closely related to their size, morphology and the types of composites. Therefore, it was important to prepare novel Ag nanostructures with superior function. Ag nanoparticles [26], nanowires [27], nanoplates [28], hollow hierarchical microspheres [29,30] have all been reported as sensing materials for developing H_2O_2 electrochemical sensors. However, to the best of our knowledge, up to now, no branch-truck Ag nanostructures have been reported for this purpose. Branch-trunk Ag hierarchical nanostructures provide a very high electrochemically active area and thereby lead to high detection sensitivity. They could also act as enhanced elements for effectively accelerating the electron transfer between the electrode and probe molecules, which would lead to a rapid current response and in the meantime reduce the overpotential of electrochemical reactions.

In this paper, we report the synthesis of branched-truck hierarchical nanostructures containing Ag nanowire trunks and Ag nanorod branches by a simple two-step synthesis pathway. High-quality single crystalline Te nanowire backbones were synthesized using a hydrothermal approach, whereas Ag nanorod branches were subsequently grown perpendicularly to the axis of Te nanowires via microwave-assisted synthesis (EG as solvent and reducing agent, PVP as polymer surfactant and $CuCl_2$ as control agent). The as-prepared branched-truck hierarchical nanostructure-modified electrode was used as a novel high-performance H_2O_2 sensor. The experimental data illustrated that the branch-truck Ag hierarchical nanostructure-modified electrodes demonstrated excellent catalytic performance for H_2O_2 reduction, while detection with a wide linear range, good selectivity and long-term stability was achieved.

2. Experimental

2.1. Materials

$K_3Fe(CN)_6$, $K_4Fe(CN)_6$, ammonium hydroxide, acetone, hydrazine (50%), KH_2PO_4, K_2HPO_4 were purchased from Tianjin Damao Chemical Factory (Tianjin, China). PVP [poly-(*N*-vinyl-2-pyrrolidone)] was obtained from Sigma-Aldrich (Darmstadt, Germany), $AgNO_3$, Na_2TeO_3 and H_2O_2 was obtained from Xiya Reagent (Chengdu, China). All the chemicals were of analytical grade. Distilled water was used in the experiments.

2.2. Apparatus

The electrochemical experiments were performed using a CHI660D electrochemical workstation (Chenhua, Shanghai, China). A standard three-electrode system (Ag branch-trunk hierarchical nanostructures modified electrode as work electrodes, Pt as the counter electrode and Ag/AgCl (saturated KCl) as reference electrode) was used in all the experiments. Scanning electron microscopy (SEM) analyses were performed using a 6701F instrument (JEOL, Tokyo, Japan). X-ray diffraction (XRD) analysis was carried out on an Ultima IV X-ray diffractometer (Rigaku, Tokyo, Japan). A microwave oven with 10–500 W power was used.

2.3. Synthesis of Branch-Truck Ag Hierarchical Nanostructures

Te nanowires were synthesized according to the reference [31]. Briefly, 1.0 g PVP and 0.0922 g of sodium tellurite were dissolved in 35 mL of double-distilled water to form a homogeneous solution

under vigorous magnetic stirring at room temperature. Then 1.65 mL of hydrazine hydrate and 3.35 mL of aqueous ammonia solution were added into the previous solution. The final solution was transferred into a Teflon-lined stainless steel autoclave (50 mL in total volume), which was closed and maintained at 180 °C for 4 h, and then the sample was allowed to cool to room temperature. 110 mL of acetone was added into the final solution to precipitate the product, which was then centrifuged and washed with double-distilled water and absolute ethanol several times, respectively. Synthesis of branch-truck Ag hierarchical nanostructure: in brief, 15 mL of 1 mM $CuCl_2$/EG was prepared firstly. Then, 1.27 mg of Te nanowires and 1 g PVP was added into the above solution, followed by the addition of 5 mL of 20 mM $AgNO_3$/EG solution. The resulting solution was then transferred to a microwave for heating reaction at (temperature). After the reaction, the solution was cooled to room temperature. The final product was obtained, in order to remove the remaining $CuCl_2$, EG and PVP, after the solution was centrifuged and washed in acetone, alcohol and deionized water at a speed of 9000 r/min for 5 min each, respectively.

2.4. Fabrication of Branch-Truck Ag Hierarchical Nanosturture Sensor

First, bare glass electrode (GCE) was polished on suede with 1.0 and 0.3 μm Y-Al_2O_3 powder, respectively. The electrodes were washed with ethanol and double distilled water for 20 min, and then the performance of bare glass electrodes were detected in $K_3Fe(CN)_6$/$K_4Fe(CN)_6$. 1 mg branch-truck Ag hierarchical nanostructures were dispersed in 1 mL Nafion solution (1%) for 10 min. The suspension solution was dispersed onto a GCE surface with a microsyringe and dried at room temperature.

3. Results and Discussion

3.1. Characterization

Te nanowires were used as substrate and templates to prepare the branch-truck Ag hierarchical nanostructures. Figure S1 shows the SEM image of the as-prepared Te nanowires with a diameter of several hundred nanometers. XRD patterns of the Te nanowires were showed in Figure S2. All peaks can be indexed with the standard JCPDS card no. 36–1452 which confirms the hexagonal phase of tellurium nanowires. The peaks observed at 2θ values of 23.08°, 27.72°, 38.36°, 40.52°, 43.44°, 45.98°, 46.92°, 49.63°, 56.82°, 62.78°, 63.93°, 65.72°, 67.64°, 71.92°, and 75.24° are assigned to the diffractions from (100), (101), (102), (110), (111), (003), (200), (201), (202), (113), (210), (211), (104), (212) and (304) planes, respectively. Figure S3 show cyclic voltammograms of Te nanowires modified electrode in PBS solution with scan rate of 50 mVs^{-1}. A pair of sharp redox peaks at +0.264 V and −0.74 V are due to the self-redox of Te nanowires [32].

3.2. The Influence of Synthesis Condition:

When Te nanowires were used as precursor and template, the hierarchical Ag nanostructure was obtained via microwave-assisted synthesis by adjusting the synthetic parameters. In the presence of PVP and $CuCl_2$, the microwave power was set at 300 W and the reaction time was set at 30 s, Te-Ag core shell nanowire backbones were found to be fully covered by Ag thin layers with abundant flake-like Ag nanostructures (Figure 1A,B).

When the reaction time was prolonged to 60 s, complete nanorods with about 50–80 nm in width and 100–300 nm in length grew perpendicularly on the surface of the nanowires (Figure 1C,D). We further increased the reaction time to 90 s, and the branched Ag nanostructure was still growing in size. Ag nanorods eventually completely covered the nanowire backbones to form branch-stem Ag hierarchical nanostructures with an average diameter of ca. 100 nm and lengths of several hundreds of nanometers (Figure 1E,F). When the microwave power was set at 500 W and the microwave time was set at 90 s, vertical nanoplates will spring out of the Ag nanowire backbones to form Ag nanoplates on the surface of Te nanowire structures (Figure S4A,B). Vertical nanoplates can be generated either sparsely or densely by increasing the number of platelets at higher growth temperatures and lower

pressures [33]. In the absence of PVP and CuCl$_2$, when the microwave power was set at 300 W and the microwave time was set at 90 s, Ag nanoparticles with irregular sizes and shapes were found to be generated on the surface of Te nanowires whereas no nanorods were observed on the Ag nanowires backbone (Figure S5A,B). This is because PVP, as a surfactant, will direct the growth of Ag to the nanorod structure form [34–36].
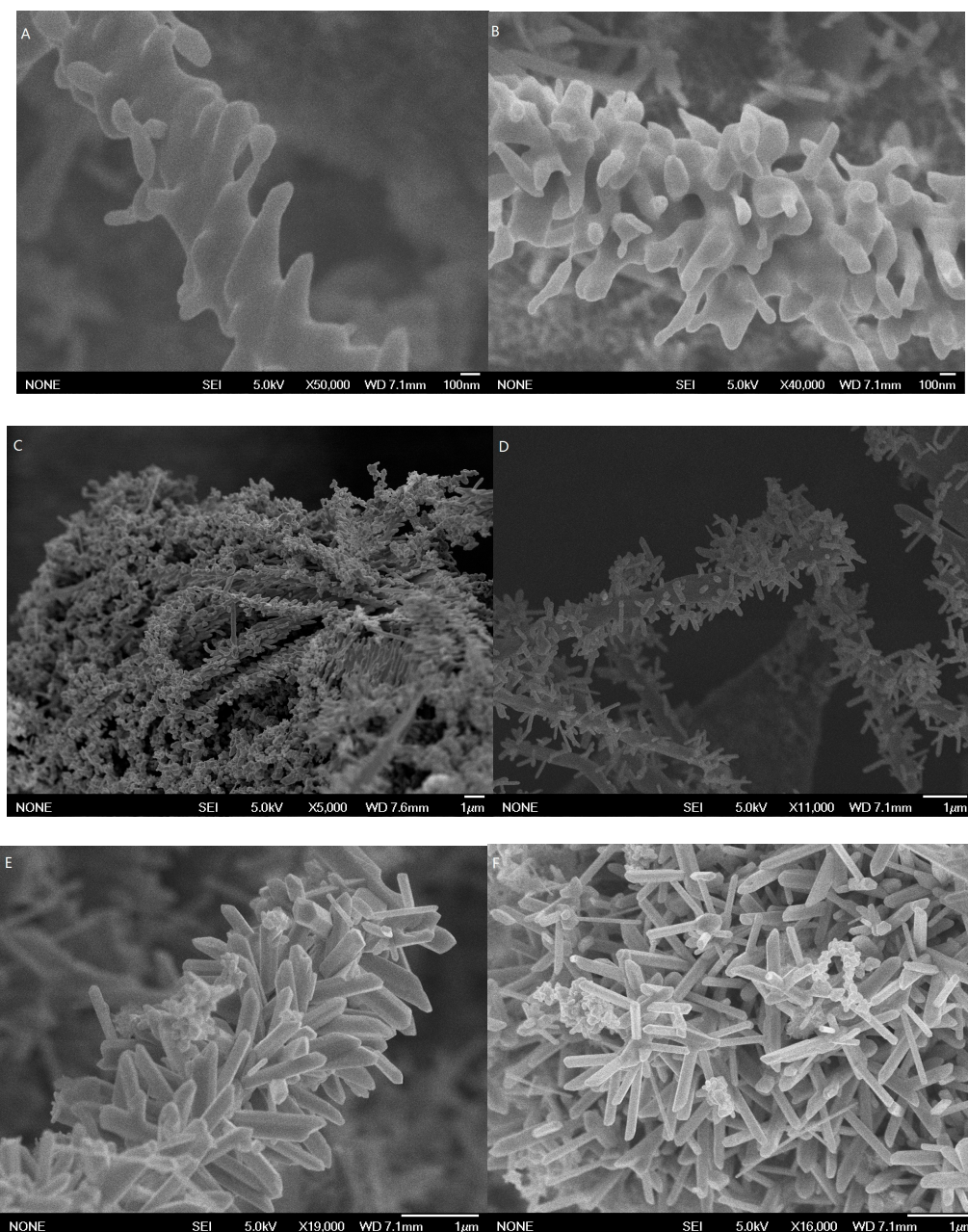
Figure 1. Typical SEM images of the branch-trunk Ag hierarchical nanostructures of different reaction time. (**A,B**) 30 s ; (**C,D**) 60 s; (**E,F**) 90 s.

The XRD patterns of as-synthesized branch-stem Ag hierarchical nanostructures with various growth times are shown in Figure 2. The XRD patterns of 60 s branch-stem Ag hierarchical nanostructures is the mixture of diffraction peak of silver and tellurium. For comparison, the peaks of 90 s branch-stem Ag hierarchical nanostructures occurring at 38.14°, 44.32°, 64.43°, 77.56°, and 81.54° were attributed to diffractions from the (111), (200), (220), (311), and (222) crystal planes, which were

consistent well with a face-centered cube of Ag. No diffraction peaks corresponding to Te were found, which suggested that the Te nanowire backbone have been completely replaced with Ag. The schematic illustration of the growth mechanism of Ag branches on the Ag nanowire backbones by microwave-assisted synthesis was shown in Figure 3.
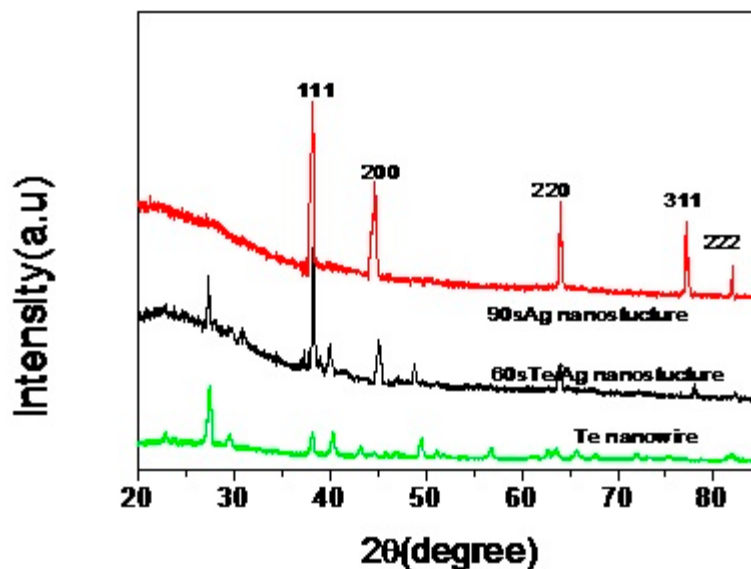

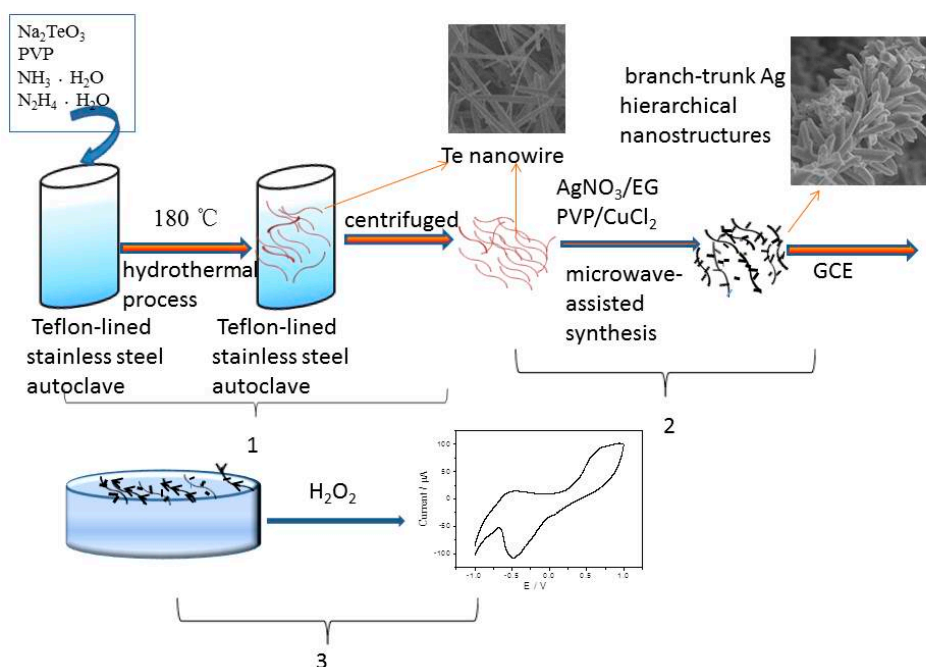**Figure 2.** XRD patterns of branch-trunk Ag hierarchical nanostructures generated at different reaction time.


Figure 3. Schematic illustration of the formation mechanism of branch-trunk Ag hierarchical nanostructures and branch-trunk Ag hierarchical nanostructure-modified GCE used for detecting H_2O_2.

An enormous amount of silver nanoparticles was synthesized via microwave-assisted synthesis. Ag cations replace Te in Te nanowires to form Ag nanoparticles at Te nanowires surface via a galvanic displacement reaction. The reaction between Te nanowires and Ag^+ can be formulated as follows:

$$Ag^+ + Te + 3H_2O = Ag + TeO_3{}^{2-} + 6H^+ \tag{1}$$
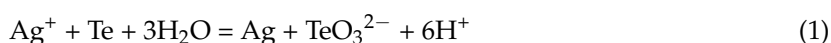
As the galvanic replacement reaction proceeded, the Ag nanoparticles would grow along Ag crystal seeds on the surface of the Ag nanowire to form nanospikes and nanoflakes. As the reaction continued, the Ag nanospikes and nanoflakes increased in size gradually and formed nanorods. Finally, high-quality Ag nanorods were produced and attached to the Ag nanowires.

Figure 4 depicts cyclic voltammograms (CVs) of bare GCE (a) and branch-truck Ag hierarchical nanostructures/GCE (b) in 0.1 M PBS (pH = 7.4) in the presence of 0.5 mM H_2O_2 with scan rate of 50 mVs^{-1}. A strong peak at about -0.48 V, attributed to the reduction of H_2O_2, was seen on branch-truck Ag hierarchical nanostructures modified GCE whereas a very small reduction peak was obtained at -0.61 V for H_2O_2 at bare GCE. The insert of Figure 4 shows the cyclic voltammogram of bare GCE in 0.1 M PBS (pH = 7.4) in the presence of 0.5 mM H_2O_2 with scan rate of 50 mVs^{-1}. Compared with bare GCE, a positively shifted peak potential of 110 mV was observed on the branch-truck Ag hierarchical nanostructures modified/GCE. There was an increase in current by increasing H_2O_2 concentration. When H_2O_2 concentration was increased from 2 mM to 8 mM, an increase reduction current was observed (Figure 5). Thus, branch-truck Ag hierarchical nanostructures could greatly reduce the overpotential and increase the catalytic current toward the reduction of H_2O_2, which was important for improving the high sensitive and selective detection for H_2O_2.
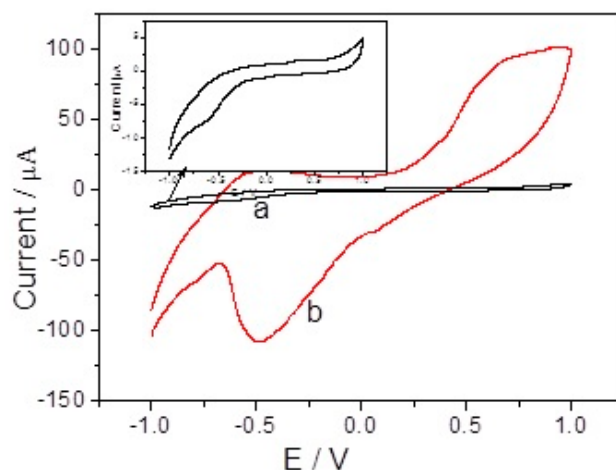
Figure 4. CVs of bare electrode (a) and branch-trunk Ag hierarchical nanostructures/GCE (b) in 0.1 M PBS (pH = 7.4) in the presence of 0.5 mM H_2O_2. Scan rate: 50 mVs^{-1}.
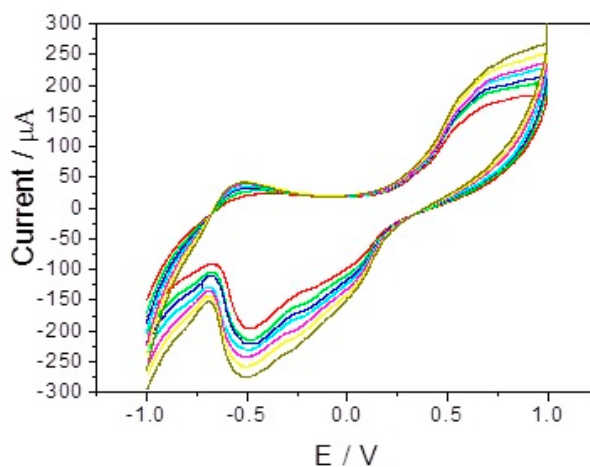

Figure 5. CVs of branch-trunk Ag hierarchical nanostructures/GCE in 0.1 M PBS (pH = 7.4) containing, 2 mM, 3 mM, 4 mM, 5 mM, 6 mM, 7 mM, 8 mM H_2O_2. Scan rate: 50 mVs^{-1}.

Direct electrochemical reduction of H_2O_2 at ordinary solid electrodes shows low electrode kinetics and high overpotential. Based on the available literature, the mechanism of H_2O_2 electroreduction can be described as follows [37]:

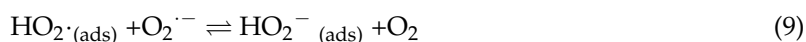$$OH\ (aq) + e^- \rightleftharpoons OH^- \tag{2}$$

$$H_2O_2 + e^- \rightleftharpoons OH\ (aq) + OH^- \tag{3}$$

$$2OH^- + 2H^+ \rightleftharpoons 2\ H_2O \tag{4}$$

In the case of silver-catalyzed decomposition of H_2O_2, the reaction turned more irreversible [37]:

$$H_2O_2 \overset{Ag}{\rightarrow} 1/2\ O_2 + H_2O \tag{5}$$

$$O_2 + 2e^- + 2H^+ \rightarrow H_2O_2 \tag{6}$$
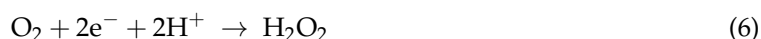
The O_2 produced in the catalytic reaction would induce detection signal on the electrode. According to some theories in the literature, the mechanism of the O_2 reduction on the electrode as described below [38,39]:

$$O_2 + e^- \rightleftharpoons [O^{\cdot -}]_{(ads)} \tag{7}$$

$$[O^{\cdot -}]_{(ads)} + H_2O \rightleftharpoons HO_2{}^{\cdot}{}_{(ads)} + OH^- \tag{8}$$

Then:

$$HO_2{}^{\cdot}{}_{(ads)} + O_2{}^{\cdot -} \rightleftharpoons HO_2{}^-{}_{(ads)} + O_2 \tag{9}$$

or:

$$HO_2{}^{\cdot}{}_{(ads)} + e^- \rightleftharpoons HO_2{}^-{}_{(ads)} \tag{10}$$
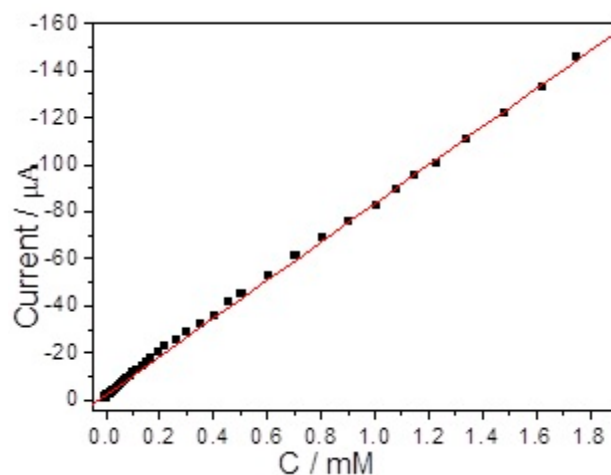
Figure 6 shows the amperometric response of the branch-truck Ag hierarchical nanostructures/GCE with gradually additions of H_2O_2 to the PBS solution under stirring conditions. As the potential was set at -0.5 V, the branch-truck Ag hierarchical nanostructures/GCE responded rapidly and achieved steady-step current by adding H_2O_2 to the solution. The insert of Figure 6 shows the low concentration range. The corresponding linear calibration curve shown in the inset of Figure 7 reveals there were a good linear relationship between the reduction peak current and the H_2O_2 concentration with the range of 0.05 μM to 1.925 mM with a correlation coefficient of 0.998. The regression equation was I (μA) = -83.18 C $-$ 2.1897 (C is the concentration of H_2O_2 in mM). The detection limit of H_2O_2 sensors was 0.013 μM (S/N = 3).

The sensitivity was calculated to be 325.52 μA mM^{-1} cm^{-2}. The as-fabricated H_2O_2 sensors were compared with those of Ag nanomaterials-based non-enzymatic H_2O_2 sensors in Table 1. The proposed method was better than the previous reports. To illustrate the feasibility in practical sample analysis of the proposed branch-truck Ag hierarchical nanostructures/GCE the determination of H_2O_2 in milk samples were studied. The real samples were diluted 10 times with water and diluted milk samples were streamed into five groups separately (S. No 1, S. No 2, S. No 3, S. No 4, S. No 5), and then different concentrations of H_2O_2 (0.01, 0.05, 0.10, 0.15, and 0.20 mM) were spiked into five groups (S. No 1, S. No 2, S. No 3, S. No 4, S. No 5) of practical samples. The chronoamperometric responses were recorded of the spiked concentration, measured concentration of H_2O_2, and relative standard deviation (RSD) (three repeated experiments). The results, listed in Table 2, showed good reliability and reproducibility for the branch-truck Ag hierarchical nanostructures/GCE.
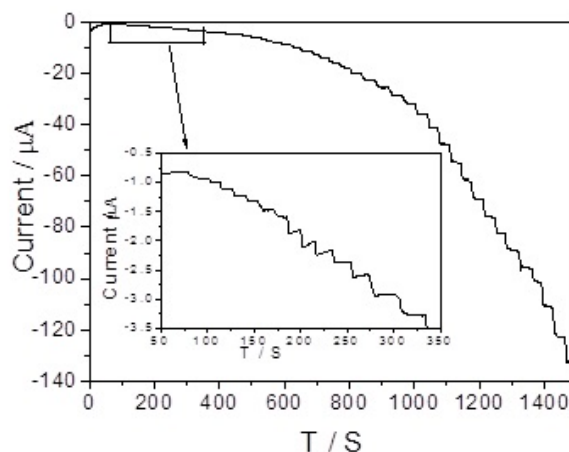
Figure 6. Amperometric response of the sensor for successive addition of H_2O_2 in N_2-saturated 0.1 M PBS (pH = 7.4) solution. The applied potential is -0.5 V, (inset: a partial magnification of the current response toward a low concentration of H_2O_2 solution).

Figure 7. The calibration curve of the amperometric response.

Table 1. Comparison of the fabricated sensor with other Ag material-based non-enzyme sensors for H_2O_2.

| Electrode	Sensitivity (μA mM^{-1} cm^{-2})	Linear Range (μM)	LOD (μM)	Ref
Ag NPs/rGO/GCE	225	50–5000	10	[40]
Ag Y/CPE	650.7	20–5000	1.4	[41]
Ag NPs/rGO/GCE	—	10–6000	1.8	[42]
Ag-Au@Cu$_2$O NWs/GCE	—	100–9000	1.1	[43]
AgNPs/SBA-16/GCE	816.6	20–8000	2.95	[44]
Ag@SiO$_2$@Ag/GCE	56.07	5–24,000	1.7	[45]
AgNPs/X-CPE	60.6	20–11,760	9.1	[26]
Ag/boehmite NTs/rGO/GCE	80.14	0.5–10,000	0.17	[46]
branch-truck Ag HN/GCE	325.52	0.05–1925	0.013	our report

Where GCE—glassy carbon electrode, CPE—carbon paste electrode, Ag NPs—Ag nanoparticles, rGO—reduced grapheme oxide, Ag Y—Ag nanoparticles arrays, Ag-Au@Cu$_2$O NWs—Cu$_2$O nanocubes decorated by Ag-Au alloy nanoparticles, SBA-16—mesoporous SBA-16 nanoparticles, Ag@SiO$_2$@Ag—Ag@SiO$_2$@Ag, X—NaX nanozeolite, boehmite NTs—Ag decorated boehmite nanotubes, branch-truck Ag HN—branch-truck Ag hierarchical nanostructures.

Table 2. The practical sample analysis result of hydrogen peroxide for the branch-truck Ag hierarchical nanostructures/GCE in pH 7 PBS (three repeated experiments).

S. No	Added Concentration (mM)	Found Concentration (mM)	Recovery (%)	RSD (%)
1	0.0100	0.01012	101.2	3.1
2	0.0500	0.05005	100.5	1.6
3	0.1000	0.09987	99.87	3.2
4	0.1500	0.15015	100.1	5.6
5	0.2000	0.01996	99.8	1.8

Where S. No 1—diluted milk sample 1, S. No 2—diluted milk sample 2, S. No 3—diluted milk sample 3, S. No 4—diluted milk sample 4, S. No 5—diluted milk sample 5.

In practical samples analysis, some coexisting biomolecules can cause serious interference in the detection of a single component. Possible interfering species for detecting H_2O_2 such as dopamine (DA), ascorbic acid (AA), glucose and uric acid (UA) were investigated by amperometric response (Figure 8) with additions of 100 µL 1 mM H_2O_2, 1 mM H_2O_2, 10 mM AA, 10 mM DA, 10 mM UA and 10 mM glucose and 200 µL 1 mM H_2O_2. The branch-truck Ag hierarchical nanostructures/GCE showed a high sensitivity amperometric response to H_2O_2 whereas there is no obvious amperometric response for the interfering species AA, glucose and UA. Additionally, the interferent DA only produces a weak reduction current at −0.5 V. Therefore, at an applied potential of −0.5 V coexistint interferents do not interfere with the selective determination of H_2O_2.
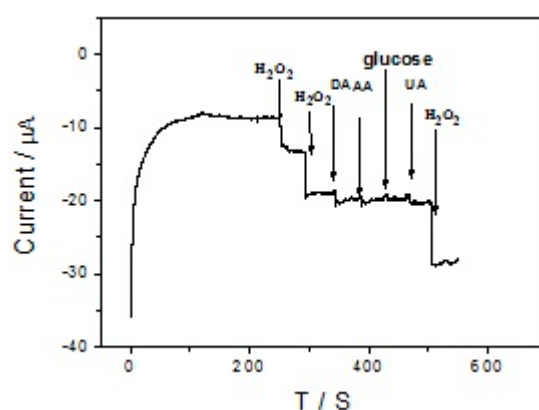
Figure 8. Amperometric curves of branch-trunk Ag hierarchical nanostructures/GCE for successive additions of H_2O_2 and different interfering substances in the 0.1 M PBS solution (pH 7.4). The applied potential is −0.5 V.

As important evaluation sensor parameters, the repeatability and stability of the H_2O_2 sensors were investigated. The branch-truck Ag hierarchical nanostructures modified electrodes were used to detect 1 mM H_2O_2 with the applied potential range of −1.0 V to 1.0 V. The catalytic current decreased to 90.5% after 10 scanning cycles, illustrating that the as-prepared sensor had highly reproducibility (Figure 9). Furthermore, the relative standard deviation (RSD) for five branch-truck Ag hierarchical nanostructures modified electrodes to detect the same 0.5 mM H_2O_2 solution was 4.1%, further indicating the good reproducibility of the branch-truck Ag hierarchical nanostructures-based H_2O_2 sensor. To study the stability of the sensor, the branch-truck Ag hierarchical nanostructures modified GCE was tested after 21 days, 90% of its initial current response was remained. These results show the sensor has satisfactory performance.
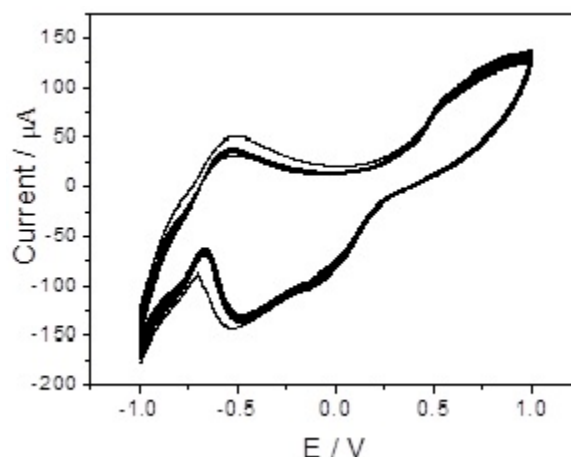
Figure 9. The repeatability of branch-trunk Ag hierarchical nanostructures/GCE in 1 mM H_2O_2 solution after 10 scanning cycles.

4. Conclusions

Branch-truck Ag hierarchical nanostructures were synthesized via a combination of hydrothermal synthesis with microwave-assisted synthesis. The as-fabricated materials could be used as an excellent charge-transfer substrate for the electrocatalytic reduction of H_2O_2. The prepared electrochemical H_2O_2 sensor showed good catalytic performance with a wide linear range, low detection limit and good selectivity and reliability. Therefore, the sensor has potential application for the selective determination of H_2O_2 in real sample analysis.

Author Contributions: Yan Zhang conceived and designed the experiments; Zhiquan Cai, Meiqiong Chen and Yan Zhang performed the experiments; Yan Zhang analyzed the data; Min Zhang and Faliang Cheng contributed reagents/materials/analysis tools; Yan Zhang and Peng Liu wrote the paper.

Conflicts of Interest: The authors declare no conflict of interest.

References

1. Zeng, G.M.; Zhang, C.; Huang, D.L.; Lai, C.; Tang, L.; Zhou, Y.Y.; Xu, P.; Wang, H.; Qin, L.; Cheng, M. Practical and regenerable electrochemical aptasensor based on nanoporous gold and thymine-Hg^{2+}-thymine base pairs for Hg^{2+} detection. *Biosens. Bioelectron.* **2017**, *90*, 542–548. [CrossRef] [PubMed]

2. Shu, S.M.; Wang, M.G.; Yang, W.; Liu, S.T. Synthesis of surface layered hierarchical octahedral-like structured Zn$_2$SnO4/SnO$_2$ with excellent sensing properties toward HCHO. *Sens. Actuators B Chem.* **2017**, *243*, 1171–1180. [CrossRef]

3. Venkadesh, A.; Radhakrishnan, S.; Mathiyarasu, J. Eco-friendly synthesis and morphology-dependent superior electrocatalytic properties of CuS nanostructures. *Electrochim. Acta* **2017**, *246*, 544–552. [CrossRef]

4. Radhakrishnan, S.; Kim, H.Y.; Kim, B.S. A novel CuS microflower superstructure based sensitive and selective nonenzymatic glucose detection. *Sens. Actuators B Chem.* **2016**, *233*, 93–99. [CrossRef]

5. Her, Y.C.; Yeh, B.Y.; Huang, S.L. Vapor−Solid Growth of p-Te/n-SnO$_2$ Hierarchical heterostructures and their enhanced room-temperature gas sensing properties. *Appl. Mater. Interfaces* **2014**, *6*, 9150–9159. [CrossRef] [PubMed]

6. Khoang, N.Y.D.; Trung, D.D.; Duy, N.V.; Hoa, N.D.; Hieu, N.V. Design of SnO$_2$/ZnO hierarchical nanostructures for enhanced ethanol gas-sensing performance. *Sens. Actuators B Chem.* **2012**, *174*, 594–601. [CrossRef]

7. Usui, Y.; Sato, K.; Tanaka, M. Catalytic dihydroxylation of olefins with hydrogenperoxide: An organic-solvent- and metal-free system. *Angew. Chem. Int. Ed.* **2003**, *42*, 5623–5625. [CrossRef] [PubMed]

8. Rojas, M.R.; Leung, C.; Whitley, D.; Zhu, Y.; Arnold, R.G.; Saez, A.E. Advanced oxidation of trace organics in water by hydrogen peroxide solar photolysis. *Ind. Eng. Chem. Res.* **2011**, *50*, 12479–12487. [CrossRef]

9. Huang, X.; Atwood, C.S.; Hartshorn, M.A.; Multhaup, G.; Goldstein, L.E.; Scarpa, R.C.; Cuajungco, M.P.; Gray, D.N.; Lim, J.; Moir, R.D.; et al. The Aβ peptide of Alzheimer's disease directly produces hydrogen peroxide throughmetal ion reduction. *Biochemistry* **1999**, *38*, 7609–7616. [CrossRef] [PubMed]

10. Chang, C.W.; Wang, M.J. Preparation of Microfibrillated Cellulose Composites for sustained release of H$_2$O$_2$ or O$_2$ for biomedical applications. *Sustain. Chem. Eng.* **2013**, *1*, 1129–1134. [CrossRef]

11. Haghighi, B.; Hamidi, H.; Gorton, L. Formation of a robust and stable film comprising ionic liquid and polyoxometalate on glassy carbon electrode modified with multiwalled carbon nanotubes: Toward sensitive and fast detection of hydrogen peroxide and iodate. *Electrochim. Acta* **2010**, *55*, 4750–4757. [CrossRef]

12. Recio, E.; Alvarez-Rodriguez, M.L.; Rumbero, A.; Garzon, E.; Coque, J.J.R. Destruction of chloroanisoles by using a hydrogen peroxide activated method and itsapplication to remove chloroanisoles from cork stoppers. *J. Agric. Food Chem.* **2011**, *59*, 12589–12597. [CrossRef] [PubMed]

13. Yamamoto, M.; Nishioka, M.; Sadakata, M. Sterilization by H$_2$O$_2$ droplets undercorona discharge. *J. Electrostat.* **2002**, *55*, 173–187. [CrossRef]

14. Choudhury, N.A.; Raman, R.K.; Sampath, S.; Shukla, A.K. An alkaline direct borohydride fuel cell with hydrogen peroxide as oxidant. *J. Power Sources* **2005**, *143*, 1–8. [CrossRef]

15. Hasegawa, S.; Shimotani, K.; Kishi, K.; Watanabe, H. Electricity generation from decomposition of hydrogen peroxide. *Electrochem. Solid State Lett.* **2005**, *8*, A119–A121. [CrossRef]

16. Thome-Duret, V.; Reach, G.; Gangnerau, M.N.; Lemonnier, F.; Klein, J.C.; Zhang, Y.; Hu, Y.; Wilson, G.S. Use of a subcutaneous glucose sensor to detect decreases in glucose concentration prior to observation in blood. *Anal. Chem.* **1996**, *68*, 3822–3826. [CrossRef] [PubMed]

17. Duff, D.G.; Baiker, A.; Edwards, P.P. A new hydrosol of gold clusters. 1. Formation and particle size variation. *Langmuir* **1993**, *9*, 2301–2309. [CrossRef]

18. Liu, Q.Y.; Zhu, R.R.; Du, H.; Li, H.; Yang, Y.T.; Jia, Q.Y.; Bian, B. Higher catalyticactivity of porphyrin functionalized Co$_3$O$_4$ nanostructures for visual and colorimetric detection of H$_2$O$_2$ and glucose. *Mater. Sci. Eng. C* **2014**, *43*, 321–329. [CrossRef] [PubMed]

19. Dickinson, B.C.; Chang, C.J. A targetable fluorescent probe for imaging hydrogen peroxide in the mitochondria of living cells. *J. Am. Chem. Soc.* **2008**, *130*, 9638–9639. [CrossRef] [PubMed]

20. Yue, H.F. Quantitative determination of trace levels of hydrogen peroxide incrospovidone and a pharmaceutical product using high performance liquid chromatography with coulometric detection. *Int. J. Pharm.* **2009**, *375*, 33–40. [CrossRef] [PubMed]

21. Liu, G.D.; Lin, Y.H. Amperometric glucose biosensor based on self-assembling glucose oxidase on carbon nanotubes. *Electrochem. Commun.* **2006**, *8*, 251–256. [CrossRef]

22. Ronkainen, N.J.; Halsall, H.B.; Heineman, W.R. Electrochemical Biosensors. *Chem. Soc. Rev.* **2010**, *39*, 1747–1763. [CrossRef] [PubMed]

23. Radhakrishnan, S.; Kim, S.J. An enzymatic biosensor for hydrogen peroxide based on one-pot preparation of CeO 2-reduced graphene oxide nanocomposite. *RSC Adv.* **2015**, *5*, 44346–44352. [CrossRef]

24. Radhakrishnan, S.; Kim, S.J. Facile fabrication of NiS and a reduced grapheme oxide hybrid film for nonenzymatic detection of glucose. *RSC Adv.* **2015**, *5*, 12937–12943. [CrossRef]

25. Zhang, M.; Zhang, Y.; Liu, P.; Chen, M.Q.; Cai, Z.Q.; Cheng, F.L. Template Control Preparation of High-Density and Large-Area Ag Nanowire Array and H$_2$O$_2$ Determination. *Int. J. Electrochem. Sci.* **2015**, *10*, 4314–4323.

26. Li, D.; Meng, L.Y.; Dang, S.C.; Jiang, D.L.; Shi, W.D. Hydrogen peroxide sensing using Cu$_2$O nanocubes decorated by Ag-Au alloy nanoparticles. *J. Alloys Compd.* **2017**, *690*, 1–7. [CrossRef]

27. Park, J.S.; Kim, J.H.; Na, J.Y.; Kim, D.H.; Kang, D.; Kim, S.K.; Seong, T.Y. Ag nanowire-based electrodes for improving the output power of ultraviolet AlGaN-based light-emitting diodes. *J. Alloys Compd.* **2017**, *703*, 198–203. [CrossRef]

28. Chen, Z.B.; Zhang, C.M.; Wu, Q.; Li, K.; Tan, L.L. A Novel application of triangular silver nanoplates forcolorimetric detection of H_2O_2. *Sens. Actuators B Chem.* **2015**, *220*, 314–317. [CrossRef]

29. Yan, T.J.; Yan, X.Y.; Guo, R.R.; Zhang, W.N.; Li, W.J.; You, J.M. Ag/AgBr/BiOBr hollow hierarchical microspheres with enhanced activity and stability for RhB degradation under visible light irradiation. *Catal. Commun.* **2013**, *42*, 30–34. [CrossRef]

30. Wang, X.L.; Yin, H.Y.; Nie, Q.L.; Wu, W.W.; Zhang, Y.; Yuan, Q.L. Hierarchical Ag/AgCl-TiO$_2$ hollow spheres with enhanced visible-light photocatalytic activity. *Mater. Chem. Phys.* **2017**, *185*, 143–151. [CrossRef]

31. Qian, H.S.; Yu, S.H.; Gong, J.Y.; Luo, L.B.; Fei, L.F. High-Quality Luminescent Tellurium Nanowires of Several Nanometers in Diameter and High Aspect Ratio Synthesized by a Poly(Vinyl Pyrrolidone) -Assisted Hydrothermal Process. *Langmuir* **2006**, *22*, 3830–3835. [CrossRef] [PubMed]

32. Zhang, A.H.; Yu, S.J.; Jiang, Y.M.; Jia, L.P.; Xia, X.H.; Ye, W.H.; Wang, C.M. A novel Pt@Te-reduced graphene oxide/polyimide composite catalyst for hydrogen evolution. *Int. J. Hydrogen Energy* **2015**, *40*, 16238–16247. [CrossRef]

33. Keuleyan, S.; Wang, M.J.; Chung, F.R.; Commons, J.; Koski, K.J. A Silicon-Based Two-Dimensional Chalcogenide: Growth of Si$_2$Te$_3$ Nanoribbons and Nanoplates. *Nano Lett.* **2005**, *15*, 2285–2290. [CrossRef] [PubMed]

34. Sun, Y.G.; Mayers, B.; Herricks, T.; Xia, Y.N. Polyol Synthesis of Uniform Silver Nanowires: A Plausible Growth Mechanism and the Supporting Evidence. *Nano Lett.* **2003**, *3*, 955–960. [CrossRef]

35. Zeng, X.P.; Zhou, B.P.; Gao, Y.B.; Wang, C.; Li, B.; Yeung, C.Y.; Wen, W.J. Structural dependence of silver nanowires on polyvinyl pyrrolidone (PVP) chain length. *Nanotechnology* **2014**, *25*, 495601–495606. [CrossRef] [PubMed]

36. Chen, D.P.; Qiao, X.L.; Qiu, X.L.; Chen, J.G.; Jiang, R.Z. Convenient, rapid synthesis of silver nanocubes and nanowires via a microwave-assisted polyol method. *Nanotechnology* **2010**, *21*, 025607–025614. [CrossRef] [PubMed]

37. Honda, M.; Kodera, T.; Kita, H. Electrochemical behavior of H_2O_2 at Ag in HClO$_4$ aqueous solution. *Electrochim. Acta* **1986**, *31*, 377–383. [CrossRef]

38. Downard, A.J. Electrochemically assisted covalent modification of carbon electrodes. *Electroanalysis* **2000**, *12*, 1085–1096. [CrossRef]

39. Šljukić, B.; Banks, C.E.; Compton, R.G. An overview of the electrochemical reduction of oxygen at carbon-based modified electrodes. *J. Iran. Chem. Soc.* **2005**, *2*, 1–25. [CrossRef]

40. Wang, M.Y.; Shen, T.; Wang, M.; Zhang, D.G.; Chen, J. One-pot green synthesis of Ag nanoparticles-decorated reduced graphene oxide for efficient nonenzymatic H_2O_2 biosensor. *Mater. Lett.* **2013**, *107*, 311–314. [CrossRef]

41. Ramezani, H.; Azizi, S.N.; Hosseini, S.R. NaY zeolite as a platform for preparation of Ag nanoparticles arrays in order to construction of H_2O_2 sensor. *Sens. Actuators B Chem.* **2017**, *248*, 571–579. [CrossRef]

42. Nia, P.M.; Lorestani, F.; Meng, W.P.; Alias, Y. A novel non-enzymatic H_2O_2 sensor based on polypyrrole nanofibers–silver nanoparticles decorated reduced graphene oxide nanocomposites. *Appl. Surf. Sci.* **2015**, *332*, 648–656.

43. Azizia, S.N.; Ghasemi, S.; Samadi-Maybodi, A.; Ranjbar-Azad, M. A new modified electrode based on Ag-doped mesoporous SBA-16 nanoparticles as non-enzymatic sensor for hydrogen peroxide. *Sens. Actuators B Chem.* **2015**, *216*, 271–278. [CrossRef]

44. Hao, H.; Sheng, Q.L.; Zheng, J.B. One-step synthesis of Ag@SiO$_2$@Ag nanomaterial and its applicationas hydrogen peroxide sensor. *Colloids Surf. A* **2017**, *518*, 124–129. [CrossRef]

45. Azizi, S.N.; Ghasemi, S.; Kavian, S. Synthesis and characterization of NaX nanozeolite using stem sweep as silica source and application of Ag-modified nanozeolite in electrocatalytic reduction of H_2O_2. *Biosens. Bioelectron.* **2014**, *62*, 1–7. [CrossRef] [PubMed]

46. Zhao, C.L.; Zhang, H.F.; Zheng, J.B. A non-enzymatic electrochemical hydrogen peroxide sensor based on Ag decorated boehmite nanotubes/reduced grapheme oxide nanocomposites. *J. Electroanal. Chem.* **2017**, *784*, 55–61. [CrossRef]